J. Fluid Mech. (2003), *vol.* 489, *pp.* 325–344.
DOI: 10.1017/S0022112003005020 Printed in the United Kingdom

Grid turbulence in shallow flows

By W. S. J. UIJTTEWAAL[1] AND G. H. JIRKA[2]

[1]Delft University of Technology, Faculty of Civil Engineering and Geosciences,
P.O. Box 5048, 2600 GA Delft, The Netherlands
W.Uijttewaal@citg.tudelft.nl

[2]University of Karlsruhe, Institute for Hydromechanics, Kaiserstrasse 12, Karlsruhe, Germany

(Received 28 October 2002 and in revised form 31 March 2003)

Results of experiments on decaying turbulence in shallow water flow bounded by a solid bottom and a free surface are presented. The evolution of the turbulence structures generated by a grid, with horizontal mesh dimensions larger than the water depth, is measured using laser Doppler velocimetry and particle image velocimetry (PIV). The vertical confinement of the flow forces the large turbulence structures to move in the horizontal plane, thus attaining strongly two-dimensional features. This two-dimensionality and its consequences for the intensities and length scales of the large structures are analysed. It is shown that the decay of the vortices that are shed from the grid is determined by the characteristic size of the grid elements rather than the grid spacing. Furthermore, during the decay process the merging of vortices is observed in combination with a -3 slope in the energy density spectrum of the velocity fluctuations. Using the PIV data, spatial properties like divergence and enstrophy can be derived for the velocity field near the free surface. The distinct effect of water depth that is found in the velocity fluctuations is almost insignificant in the enstrophy decay.

1. Introduction

Shallow flows are omnipresent in the natural environment. From stratified atmospheric flows to flows in rivers and coastal areas, where the vertical dimension is much smaller than the horizontal, the geometry forces its signature on the turbulence properties. In these cases and others where stratification or background rotation play a role, the flow exhibits strong two-dimensional behaviour. In contrast to the large space available for the turbulence motions in the horizontal plane, the vertical confinement suppresses vortex stretching, an important dissipation mechanism. Many studies are therefore dedicated to pure two-dimensional turbulence.

However, in most practical cases three-dimensional influences are present, affecting the evolution of the large-scale turbulent motion by additional frictional dissipation at the confining boundaries or even destroying the two-dimensionality by strong vertical mixing. A number of experiments on shallow jets, wakes and mixing layers have shown that under certain conditions the turbulence properties are strongly affected by the two-dimensionality while a change in e.g. water depth can result in dramatic changes towards full three-dimensionality. In order to develop and improve modelling tools that are able to cope with these phenomena, experimental data are invaluable.

1.1. *Turbulence in shallow flows*

In experiments on shallow jets Dracos, Giger & Jirka (1992) showed that the turbulence properties of a plane jet in deep water differ significantly from those under

shallow conditions. The vertical confinement of the flow allows two-dimensional instabilities to grow without being destroyed by three-dimensional instabilities. This results in a high-Reynolds-number jet with the properties of a two-dimensional jet at a much lower Reynolds number.

Similar phenomena were found for shallow wake flows (Chen & Jirka 1995) and shallow mixing layers (Uijttewaal & Booij 2000). The occurrence of large-scale eddies in those cases is associated with one-dimensional energy spectra containing a pronounced peak with a clear -3 slope, a feature that is absent in wind-tunnel grid turbulence but clearly present in two-dimensional flows.

A qualitative explanation for these phenomena is that when the energy-containing large eddies have attained dimensions larger than the water depth, the small-scale turbulence generated in the bottom boundary layer has little effect on those eddies and can only act as a kind of small-scale eddy viscosity. The basic turbulence dissipation mechanism of vortex stretching does not apply anymore to the large eddies. Moreover, interpreting the small-scale eddy viscosity as an effective viscosity, Reynolds numbers thus formed become orders of magnitude smaller, leading to phenomena like periodic vortex shedding that would not be possible for the conventional Reynolds number based on the molecular viscosity.

The interpretation described above does not explain the mechanism by which the large structures are formed. In flows with well-defined regions of mean shear, linear stability analysis offers the possibility to predict the onset of large-scale fluctuations (van Prooijen & Uijttewaal 2002). It is however not clear how these large-scale fluctuations develop further. From the fluctuations, vortices might develop, which can grow to larger scales by viscous interaction or by the mechanism of vortex pairing. It is therefore interesting to see whether similar phenomena occur in homogeneous shallow flows, i.e. flows without mean velocity gradients in the horizontal plane. This configuration can be achieved by positioning a grid in a uniform wide channel flow. The grid should be constructed such that the induced turbulence senses the shallowness of the flow. It is expected that the turbulence properties in such a flow are governed by the vortex dynamics itself and not by mean flow properties like transverse shear.

In studying two-dimensional turbulence, grids have often been used to induce turbulence fluctuations. A short overview will therefore be given on previous work concerning decaying grid turbulence in connection with two-dimensional flows.

1.2. *Two-dimensional turbulence*

Since the pioneering work by Fjortoft (1953), Batchelor (1969) and Kraichnan (1967), many scientists have sought an experimental proof of the numerically predicted energy density spectra. The signature of forced two-dimensional turbulence is two-fold. When the forcing takes place at a certain frequency f_0, a $-5/3$ slope in the spectrum develops at the low-frequency side of f_0, representing energy scaling. This specific slope indicates that energy is transferred from the forcing frequency into the larger-scale turbulent motion. In analogy with the well-known energy cascade towards smaller scales in three-dimensional turbulence, this process is named inverse or reverse energy cascading. Fluctuations induced by the forcing have the tendency to organize into large-scale eddies. Though this self-organizing process has frequently been observed, obtaining an unquestionable proof of the $-5/3$ slope in the energy density spectrum has turned out to be far from obvious. Recent experimental work by Paret & Tabeling (1997) demonstrates the presence of a substantial interval of the

spectrum with the predicted slope. Such experiments are not easily performed due to the difficulty of creating a continuously forced two-dimensional turbulent flow.

The part of the spectrum with length scales smaller than those of the forcing reflects the transfer of energy toward smaller scales down to the dissipative scales. This part of the spectrum represents the small-scale vorticity filaments separating neighbouring eddies of opposite vorticity. In fact the requirement of enstrophy conservation valid for inviscid flows demands that the small-scale vorticity is increased simultaneously with the inverse cascade of vorticity into the large scales. The slope of the energy-density spectrum associated with this down-cascading has the value of -3, representing enstrophy scaling.

In grid turbulence the energy is injected at the location of the grid, from where the turbulent kinetic energy is advected while decaying. This decaying process does not have to obey the above-described energy transfer since the energy is not supplied continuously by the mean shear. The coarsening of the vorticity field due to the merging of vortices has been observed in a number of laboratory experiments and numerical simulations of decaying two-dimensional turbulence (Chasnov 1997; Martin, Wu & Goldburg 1998; Vorobieff, Rivera & Ecke 1999), in all cases associated with a spectral slope of -3. It should be noticed here that the process of decay in this part of the spectrum, i.e. the energy transfer towards smaller scales, follows an enstrophy scaling which means that for these length scales the vortex stretching mechanism, which is dominant in three-dimensional turbulence, is absent. Numerical simulations show that at sufficiently high Reynolds numbers the lowest-frequency part of the spectrum has a $+3$ slope (Chasnov 1997) representing the nonlinear back-scattering of energy (Lesieur 1990).

1.3. *Suppression of three-dimensionality*

Experimentally, three-dimensionality always plays an important role. The best that can be achieved is to partially suppress velocity fluctuations normal to the plane of the flow. An interesting configuration in this respect is the flow in soap films (Vorobieff *et al.* 1999). Despite small effects of thickness variation and air drag, the flow can be considered as ideally two-dimensional and is well suited for fundamental studies.

Investigating the flow of mercury in a magnetic field is an alternative way to enforce two-dimensionality (Sommeria 1986). A flow can be induced by applying electric currents. Despite some dissipation due to wall friction, the signature of an inverse energy cascade could be observed. The same principle of electromagnetic forcing can be used to drive the flow in a thin layer of NaCl-solution (Paret & Tabeling 1997). Suppressing the vertical fluctuations by density stratification has often been successfully applied in studying the decay of turbulent motions excited by a moving objects (e.g. a grid) (Riley & Lelong 2000). Stratified flows are more common in the natural environment and the experimental findings are applicable to understanding atmospheric and oceanic flows in which stratification plays an important role (Fincham, Maxworthy & Spedding 1996).

On smaller scales like river or estuarine flows, where stratification and rotation of the Earth do not play an important role, the effect of shallowness is reflected in a combination of suppression of vertical motions due to the confinement by the water depth and a high dissipation due to the small-scale turbulence induced by the vertical velocity gradient. It is therefore relevant to seek insight into the way that small-scale three-dimensional turbulence interacts with the large-scale quasi-two-dimensional motion, since in almost every practical flow dissipation induced by wall friction and small-scale turbulence is of importance.

The suppression of three-dimensionality is also apparent near a free surface (Sarpkaya 1996; Walker, Leighton & Garza-Rios 1996), where the stresses are highly anisotropic and tangential vorticity cannot exist. In free-surface channel flow this leads to the formation of attached vortices when upwellings impinge upon the free surface (Pan & Banerjee 1995; Kumar, Gupta & Banerjee 1998). In terms of the Reynolds-stress anisotropy tensor (Lumley 1978) the small-scale turbulence is close to isotropy at half the water depth with a tendency towards two-dimensionality near the free surface and the bottom (Pope 2000). For the large-scale motions (larger than the water depth) two-dimensionality prevails.

1.4. *Objectives*

This study focuses on the evolution of structures much larger than the water depth which sense the vertical restriction, whereas the details of the connection and disconnection of vortices at the free surface (Willert & Gharib 1997) are considered as part of the small-scale turbulence. Although it is clear that the near-surface effects are important for the dynamics of the small-scale turbulence their effects on the large-scale motion are likely to be small. The main action of the small-scale turbulence is considered as dissipative. It is therefore expected that even with e.g. two no-slip walls the vertical confinement provides the conditions of forced horizontal motion for the large structures. In that case the increased friction and dissipation would lead to a faster disappearance of the large-scale motions which makes such a configuration less suitable for our purpose.

The phenomena are studied in a simple and straightforward set-up, where the emphasis is on the evolution of large horizontal structures rather than on the generation of excess turbulence with strong three-dimensional features in the near field of the grid.

Revealing the dynamics of large-scale vertically confined turbulence will contribute to the development of new modelling approaches such as are being developed for e.g. applications in river engineering and the modelling of coastal zones.

2. Experiments

The experiment starts with a fully turbulent laterally uniform and vertically sheared shallow base flow. This base flow is then disturbed by a grid formed by obstacles in the form of vertical cylinders that are uniformly distributed over the cross-section of the flow. Downstream of the grid the grid-induced turbulence will decay under the influence of the bottom friction and associated small-scale turbulence.

2.1. *Flow facility and grid configurations*

The experiments were performed in the shallow flow facility at the Institute for Hydromechanics at the University of Karlsruhe, figure 1. The basin of 13.5 m length and 5.48 m width allows water depths up to 0.25 m. The bottom is horizontal and flat with variations less than ± 1 mm. The water is circulated using a closed circuit system in which the velocity and water depth can be regulated independently. By monitoring the water level and discharge, the mean flow velocity could be kept constant and was repeatable within 3%. The large width of the basin (24 to 100 times the water depth) ensures the absence of sidewall effects and provides a laterally homogeneous flow (Carmer, Koch & Jirka 2000). In this set-up the mean flow properties vary only over the longitudinal (x) and vertical coordinates (z) without shear or preferred vorticity in the lateral direction (y). The origin of the coordinate axes was chosen at the centre of the grid in between two grid elements. The grid was made of segments of plastic

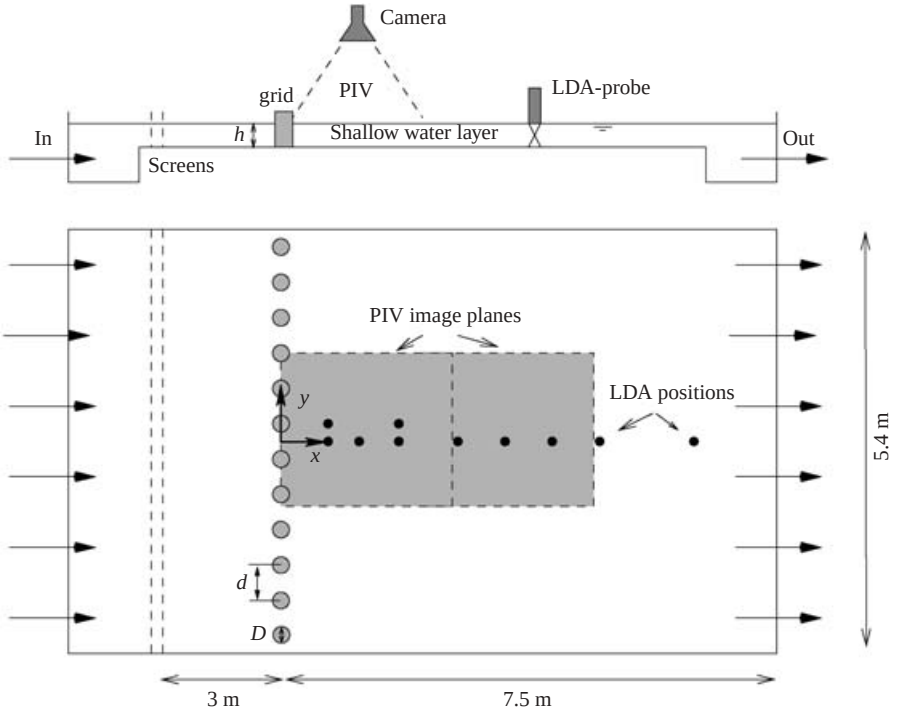

FIGURE 1. Side and top view of the experimental set-up.

tubing filled with concrete which could be accurately positioned at the bottom of the basin. With the use of a mould the spacing between the cylinders could be kept equidistant within 2% accuracy. Three types of grid elements were used: circular cylinders with diameter $D = 63$ mm (referred to as small cylinders) and 125 mm (big cylinders) respectively, and square bricks with side lengths 115 mm (square cylinders). The latter were used to investigate the influence of grid element shape and to facilitate numerical simulations that use a rectangular computational grid. With a typical mean depth-averaged velocity of $U = 0.05\,\mathrm{m\,s^{-1}}$ the Reynolds number Re_h based on the water depths of 0.045 m and 0.225 m is 2200 and 11 000 respectively. The background flow can therefore be considered fully turbulent. The Reynolds number based on the cylinder diameter ranges between 3000 and 6000. The Froude number, based on the water depth and mean velocity, was in most cases much smaller than the highest value of 0.2. This means that surface disturbances played a minor role even in the near wake of the grid cylinders. Visual inspection showed that the free surface only exhibited small vertical fluctuations < 0.5 mm over an area less than 5 cylinder diameters downstream, where three-dimensional structures could be observed between the shed vertical vortices. Further downstream the hardly noticeable free-surface disturbances looked similar to those in the undisturbed base flow upstream of the grid.

2.2. *Laser Doppler anemometry*

Laser Doppler aneomometry (LDA) measurements were performed at various distances downstream of the grid, including two extra points laterally displaced half a mesh width in order to check uniformity of the flow. A two-velocity-component *TSI-colorburst* system was used for measuring the velocity components in the horizontal

plane. With a front lens of 100 mm the dimensions of the probing volume were 1 mm in the vertical direction and 0.1 mm in the horizontal plane. The laser beams were introduced into the water from above using a small circular glass plate (diameter 50 mm), that touched the free surface. Thus the small fluctuations at the free surface directly downstream from the grid did not disturb the laser beams forming the measurement volume, while the effect of the glass plate on the flow was negligible. The surface ripple caused by the glass plate was hardly noticeable and estimated as < 0.2 mm. In all cases the measurement volume was positioned at two-thirds of the water column height, so that the bulk properties of the turbulence were measured away from the regions of high anisotropy near the bottom and the free surface (Nezu & Rodi 1986; Pan & Banerjee 1995). The boundary layer that develops along the upstream side (< 25 mm) of the glass plate is considered too thin to affect the flow at the measured location with > 15 mm depth.

The time scales of the turbulent fluctuations range from a few milliseconds for the Kolmogorov scales to tens of seconds for the expected largest structures. Of most interest for this study are the structures of the order of and larger than the water depth. In order to acquire relevant data within a frequency range that comprises the low-frequency part of the small-scale turbulence of the background flow as well as the large-scale horizontal motions, measurements were taken for 1000 s at each position with a typical mean sample rate larger than 150 Hz. This excludes the smallest scales up to a frequency of about 350 Hz, estimated from the Kolmogorov length scale. In order to reach the data rate of 150 Hz, latex particles with a diameter smaller than 10 μm were added as seeding material. As these measurements are rather time consuming (4 hours per series), the set-up is fully automated such that a complete series of measurements can be performed without intervention by the experimenter.

The irregular (not equidistant in time) data obtained with LDA were low-pass filtered and resampled at 20 Hz using a Gaussian time-window, instead of the straightforward sample-and-hold estimator, in order to allow further post-processing. The reduction in sample frequency is necessary in order to determine the high-frequency part of the power density spectra reliably (Adrian & Yao 1987).

2.3. *Particle image velocimetry*

In order to obtain more information on spatial properties like vorticity, the particle image velocimetry (PIV) technique is applied to the flow field near the free surface. For that purpose the free surface is seeded with buoyant polypropylene granulate particles with a diameter between 2 and 3 mm. With a density only slightly less than that of water, the particles are well immersed, which minimizes clustering and allows the particles to follow the large-scale, horizontal fluid motions properly. Best results were obtained by coating the particles with black paint that reduced the effects of surface tension. Since all particles move at the free surface, homogeneous indirect illumination with spotlights suffices in providing a good contrast of the black particles against the white background. Obviously the vertical fluid motions are not traced by the particles. Divergences and convergences should be minimal for the large-scale, predominantly horizontal turbulent motion. Recordings are made with a camera (PCO-Sensicam with 14 mm Nikon lens) mounted above the flume covering a plane of dimensions $1.2\,\mathrm{m} \times 1.5\,\mathrm{m}$ with a spatial resolution of 1024×1280 pixel^2 and 12-bit grey-value discrimination and 20 ms illumination time. The maximum frame rate of 7 Hz was used for the recording of 200 images in each series, thereby spanning 28.5 s. This time span was sufficient to capture the large-scale phenomena, but less suitable to determine accurate flow statistics. For that purpose the LDA data were used.

Experiment	h (m)	U ($m\,s^{-1}$)	Grid cylinder type	S (%)	d/h	D/h	Data
I	0.045	0.05	big	33	8.4	2.8	LDA,PIV
II	0.045	0.05	big	50	5.6	2.8	LDA,PIV
III	0.045	0.05	big	66	4.2	2.8	LDA,PIV
IV	0.045	0.025	big	50	5.6	2.8	LDA
V	0.045	0.05	small	33	4.2	1.4	LDA,PIV
VI	0.045	0.05	small	50	2.8	1.4	LDA,PIV
VII	0.045	0.05	small	66	2.1	1.4	LDA,PIV
VIII	0.045	0.10	small	50	2.8	1.4	LDA,
IX	0.225	0.05	small	33	0.81	0.27	LDA,PIV
X	0.225	0.05	small	50	0.54	0.27	LDA,PIV
XI	0.225	0.05	small	66	0.41	0.27	LDA,PIV
XII	0.045	0.05	square	50	5.2	2.6	LDA,PIV
XIII	0.045	0.05	square double	66	7.7	5.1	LDA

TABLE 1. Parameters for the experimental conditions.

However, by averaging over the lateral coordinate and using three independent series of PIV measurements for each location, the characteristic downstream evolution of properties like enstrophy and divergence could be determined. The recordings were made at various downstream positions, where the image areas were partially overlapping.

After removing the background noise by high-pass filtering and background subtraction, a standard PIV algorithm (DaVis 5.4.4) was applied to the recordings with 50% overlapping interrogation areas of 32×32 pixel^2 that contained on average 3 to 5 particles and resulted in a field of 64×80 vectors. In the post-processing stage erroneous vectors were removed ($< 10\%$) and replaced by the velocities based on alternative correlation peaks (when available), and by using interpolation between surrounding vectors. Obviously the resolution of the PIV technique, typically 0.05 m, was not sufficient to resolve the motions associated with the small-scale bottom turbulence. From the velocity fields the vorticity and divergence were evaluated using a central difference scheme.

2.4. *Measurements*

An overview of the parameters that were varied in the experiments is given in table 1. Not all data generated will be described here. The most important parameters of this experiment are: flow velocity U, cylinder diameter D divided by the water depth h, solidity of the grid $S = D/d$ with d denoting the distance between the centres of the grid elements. Three values of the grid solidity were used, 33%, 50% and 60%, as in numerous other grid-turbulence experiments.

3. Results

3.1. *Visual observations*

The gross features of the flow could be visualized by dye injection. Despite the diffusive character of the small-scale turbulence some features could be clearly observed. With a 33% solidity the cylinders exhibit regular vortex shedding. With 50% solidity the vortex shedding is more energetic due to the higher velocity between the cylinders and more vortex–vortex interaction is seen. At 66% a strong interaction between the cylinder wakes is observed and irregular large vortex patterns are formed directly

FIGURE 2. Dye visualization obtained for a grid with $S = 80\%$, $D = 0.125\,\mathrm{m}$, $h = 0.045\,\mathrm{m}$, $U = 0.05\,\mathrm{m\,s^{-1}}$. The area covered is $2.7\,\mathrm{m} \times 2.2\,\mathrm{m}$ with the water flowing from left to right. Dye is injected at two locations 0.47 m apart.

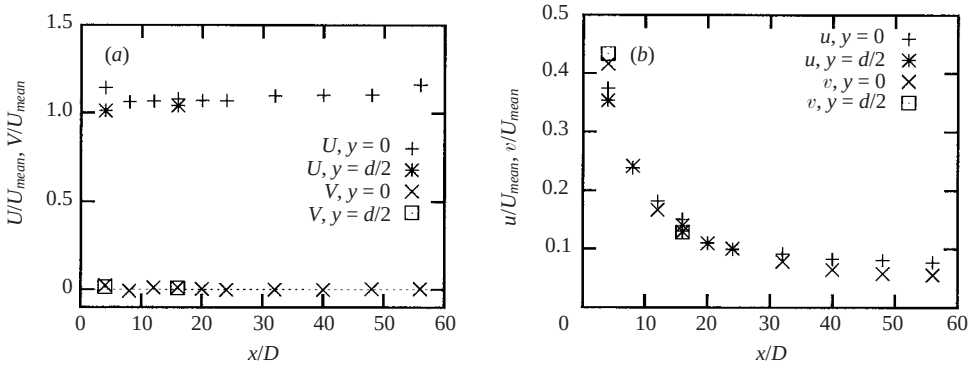

FIGURE 3. Mean (a) and standard deviation (b) of the flow velocities in the horizontal plane determined with LDA at various positions downstream, experiment II.

downstream of the grid with regions of back-flow. The depression in the free surface between the cylinders was of the order of 1 mm in this case.

In order to obtain an exaggerated view of the large-scale structures that are formed, a visualization is shown in figure 2 for the rather extreme case of 80% solidity, where dye is injected at two locations. The dimensions of the large-scale motion are an order of magnitude larger than the water depth, resulting in a fast, lateral spreading of the dye.

3.2. *Global statistics*

The LDA data were used to analyse the statistical properties of the flow downstream of the grid. Figure 3(a) demonstrates that the flow is uniform over the region of interest. Close to the grid the mean streamwise velocity U in the wake of a cylinder ($y = d/2$) is smaller than the velocity downstream of the gap between the cylinders ($y = 0$). The difference is small and appears to have no consequences for the turbulence intensities u and v. The slight increase downstream of the mean velocity is related

to the development of the vertical velocity distribution and the gradually decreasing water depth in the basin with a nominally horizontal bottom. From figure 3(*b*) it is seen that the turbulence in the lateral v and streamwise u directions is virtually isotropic. Beyond a distance of $30\,D$ the grid-induced turbulence has decayed to a level where the small-scale boundary layer turbulence becomes important and the difference between the streamwise and spanwise fluctuations is apparent. For the case shown in figure 3, the range in which the decaying turbulence can be analysed is rather short, especially when taking into account that in wind-tunnel experiments the isotropic and scalable domain starts from 20 mesh lengths (e.g. Warhaft & Lumley 1978). The relatively high background turbulence intensity confines the domain. It turns out that in this experiment the strong anisotropy and inhomogeneity is found within the first 5 cylinder diameters downstream of the grid. This leaves the restricted range between $5D$ and $30D$ for an analysis of the decay. For other parameter settings this range extends to $100D$. Given the restrictions on sampling rate and duration, the accuracy of the LDA results appears to be mainly governed by small and unavoidable imperfections in the flow geometry and discharge, and remains within one or two percent of the mean velocity.

In figure 4(*a*) the turbulent kinetic energy in the horizontal plane is depicted versus downstream position for the experimental conditions listed in table 1. The energy levels cover a range of more than three orders of magnitude with a rather consistent decaying trend. It appears that the points measured closest to the grid at 0.5 m deviate from this trend, indicating that these data are not in the regime of self-similar decay. The same data are shown in non-dimensional form in figure 4(*b*). The scaling that has been applied is based on the vortex shedding from a single cylinder, i.e. the characteristic length scale is the cylinder diameter D, and the characteristic velocity is the velocity U_c found between the cylinders $U_c = U_{mean}/(1-S)$. It is shown that the data collapse reasonably well onto a single curve. This would not have been the case if the grid spacing, which is the characteristic length scale that is commonly applied, were used. The scatter in this figure is not caused by the inaccuracy of the experiment but by a more structural deviation for the conditions of high solidity and deeper water. This is clearly seen when data for those conditions are omitted, as is done in figure 4(*c*). The remaining deviations downstream reflect the influence of the turbulence intensity that results from the bottom boundary layer. Using U_c as the characteristic velocity reveals the strongest deviation for the lowest solidities (cases I and V, $S = 33\%$). The line drawn has a slope of -1.3, a value that is commonly found in experiments on the decay of three-dimensional grid turbulence (Warhaft & Lumley 1978; George 1992). In the most simple approach of a dimensional analysis, where a single length scale determines the dissipation, the slope should be -1 (Taylor 1935), while including the energy decay in accordance with the $-5/3$ Kolmogorov law yields $-10/7$ (Comte-Bellot & Corrsin 1966). Also in experiments with soap films and strong stratification a value between -1 and -1.5 is found (Fincham *et al.* 1996; Vorobieff *et al.* 1999).

Data that deviate most over the whole range of x are shown in figures 4(*d*) and 4(*e*). It is seen that the values for 66% solidity all coincide but are structurally higher than average. This might be related to the fact that with a high solidity the flow just downstream of the grid is organized differently, i.e. regions of reversed flow occur and the jets between the cylinders have a strong interaction and appear to be dominating the flow rather than the cylinder wakes. The high turbulence intensities generated by the grid provides results in a large range downstream where the scaling holds to $100D$, and the effects of the small-scale bottom turbulence are not noticeable.

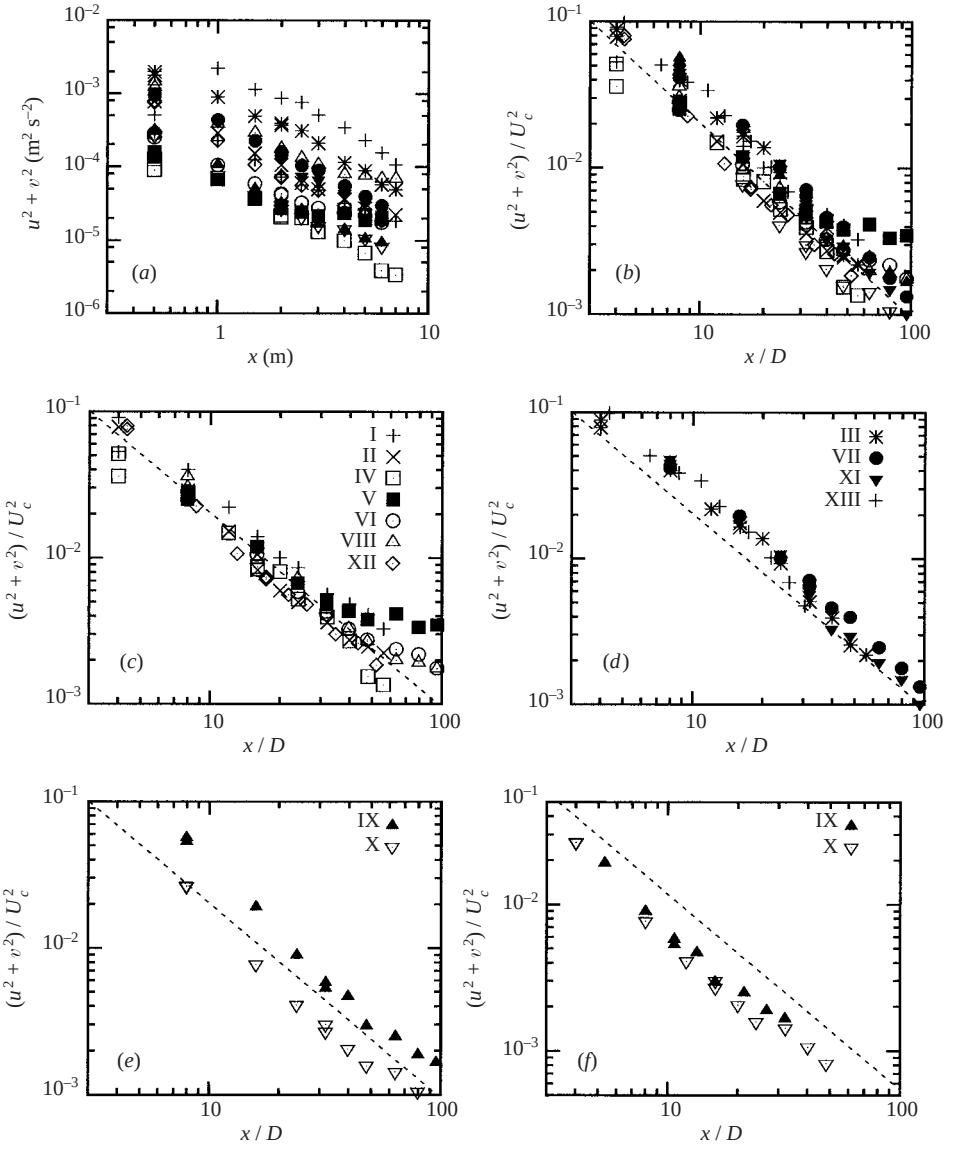

FIGURE 4. Decay of the turbulent kinetic energy as measured with LDA. The dashed line indicates a slope of -1.3, the legends refer to table 1. (*a*) All data without scaling, (*b*) all data using the proposed scaling with cylinder diameter D and velocity U_c, (*c*) data-set without experiments with $S = 66\%$ and without the data with $h = 225$ mm, (*d*) data for $S = 66\%$, (*e*) data for $h = 225$ mm, (*f*) data for $h = 225$ mm using the mesh spacing d as a scaling length.

For the relatively deep flow of 225 mm ($h = 5D$), it appears that the scaling with the cylinder diameter does not apply anymore, as shown in figure 4(*d*). In this case the mesh spacing appears a more appropriate length to scale with as demonstrated in figure 4(*f*). One might interpret this different scaling as a tendency towards a flow dominated by three-dimensional turbulence. Conversely, by confining the flow in the vertical direction the characteristic length scale changes from the common mesh spacing to the cylinder diameter. By decreasing the water depth even further, the bottom friction will directly affect the development of the large-scale motion. The

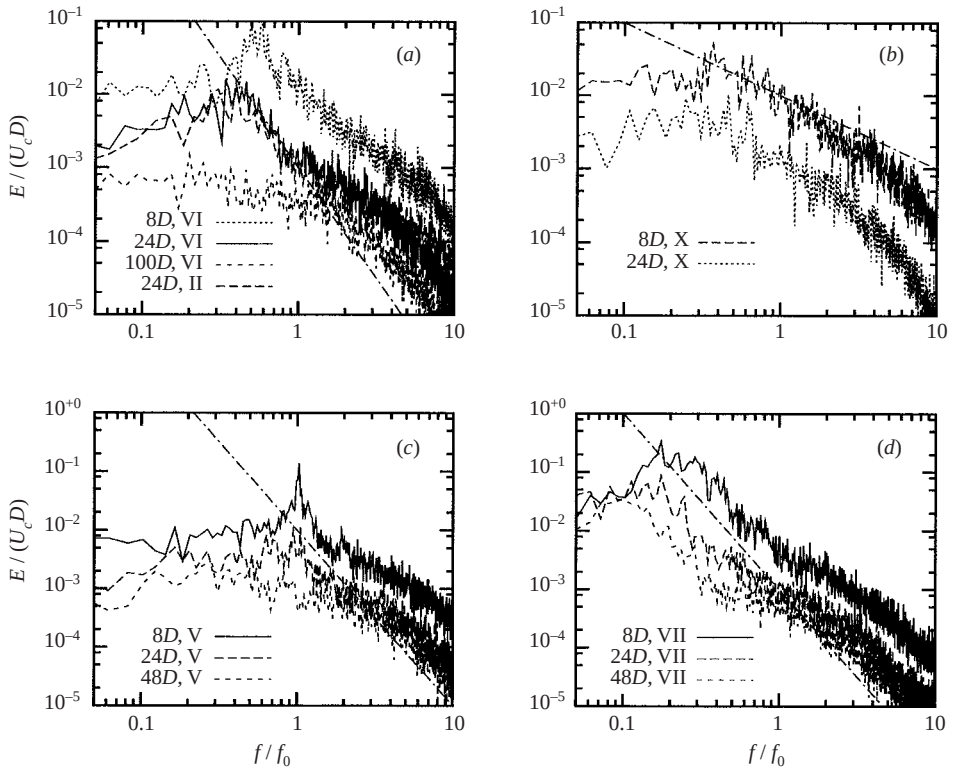

FIGURE 5. Energy density spectra for the lateral velocity component of decaying turbulence at various distances behind a grid. (*a*) 50% solidity and 45 mm water depth. The straight line indicates a -3 slope. (*b*) 50% solidity and 225 mm water depth. The straight line indicates a -1 slope. (*c*) 33% solidity and 45 mm water depth. The straight line indicates a -3 slope. (*d*) 66% solidity and 45 mm water depth. The straight line indicates a -3 slope.

distance for the frictional damping of large-scale velocity differences is then estimated by h/c_f (Dracos *et al.* 1992), in which c_f is the coefficient used in the standard quadratic law for bottom friction. The experimental conditions here yield for this length scale a minimum value of about 15 m, for a hydraulically smooth bottom with $c_f = 0.003$. The water depth should therefore be decreased more than 50% to say 20 mm in order to observe noticeable effects caused by bottom friction.

3.3. *Spectra and autocorrelations*

When studying turbulence properties, a representation in terms of energy density spectra gives an indication of the energy distribution over the various length and time scales. The process of turbulence decay can be interpreted from the shape of the spectrum. A typical example of the one-dimensional energy density spectrum obtained from this experiment is shown in figure 5(*a*). The frequency axis is scaled with the natural vortex shedding frequency for a single cylinder $f_0 = 0.2\,U_c/D$, using a Strouhal number of 0.2, whereas the energy density is scaled with $U_c\,D$. When compared with the background turbulence, as measured far from the grid where all excess turbulent kinetic energy has been dissipated, it is seen that at all frequencies the energy density is increased with a strong peak at the low-frequency side. In the decay process the peak decreases, shifting towards lower frequencies and attaining a -3 slope. This particular slope is often encountered in two-dimensional turbulence and

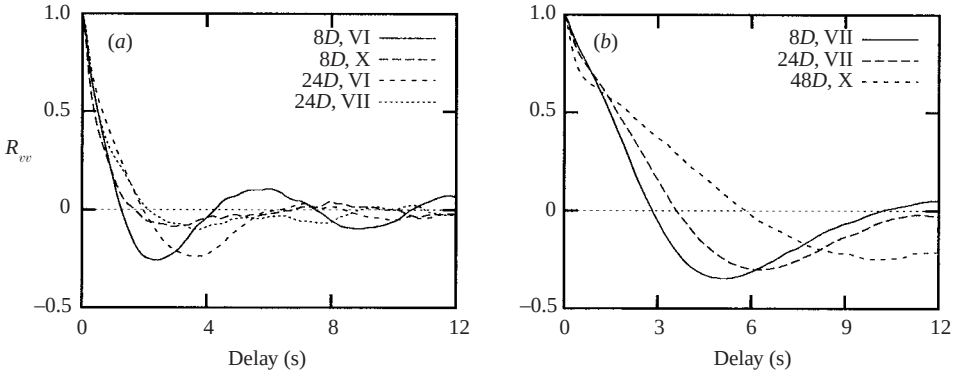

FIGURE 6. Autocorrelation functions of the lateral velocity component. (*a*) A comparison for two locations with 45 mm (case VI) and 225 mm (case X) water depth, and a grid solidity of 50%. (*b*) The large-scale modulation for the case of 66% solidity.

in shallow flows containing quasi-two-dimensional structures (Chen & Jirka 1995; Dracos *et al.* 1992; Uijttewaal & Booij 2000), although those flows always contained a mean shear which continuously supplied energy to the large-scale structures. This is an important difference with e.g. the shallow mixing layer. In the present case, the energy is decaying fast and the energy density at a certain frequency is always decreasing while the presence of mean shear would cause the energy level of the peak in the spectrum to be constant or even to increase. The present results show that in the absence of mean shear the vertical confinement is affecting the dynamics of the flow, leading to a decay process with a -3 slope in the spectrum. At higher frequencies the spectral slope tends to a much lower value close to -1. This range is related to the three-dimensional energy cascade in the neighbourhood of a wall (Perry, Henbest & Chong 1986; Nikora 1999).

This effect is clearly shown in figure 5(*b*) for the deep water cases in which clear peaks are absent and the dominating slope is close to a value of -1. At the highest frequencies shown in the graph, the slope becomes steeper indicating the start of the inertial subrange which tends to a $-5/3$ slope. Figure 5(*a*) also shows that the scaling in which the cylinder diameter has been used is appropriate, as the curves obtained for the small and the big cylinders coincide. The spectra of figure 5 deviate from the spectra commonly found for three-dimensional grid turbulence (Comte-Bellot & Corrsin 1971). In the full three-dimensional case no peak is found and the energy density monotonically decreases with a $-5/3$ slope towards higher frequencies (see e.g. Townsend 1956).

When the solidity of the grid is low the eddies that are shed from the cylinders are separated and do not have the opportunity to fully merge before they are dissipated. Figure 5(*c*) shows a sharp peak at the natural frequency f_0 at a distance $8D$, which vanishes fast at larger distances without a noticeable shift towards lower frequencies. A much stronger effect is found in the high-solidity case (66%) of figure 5(*d*). At a small distance $8D$ downstream from the grid a substantial amount of energy is already present in the low-frequency part of the spectrum. The -3 slope is convincingly clear, extending over approximately one decade. Experiments on two-dimensional turbulence in soap films and stratified flows are characterized by the same slope (Vorobieff *et al.* 1999), which is ascribed to the enstrophy cascade (Batchelor 1969).

The characteristics of the turbulence spectra can also be recognized in the autocorrelation functions of the lateral velocity components. It is seen in figure 6(*a*)

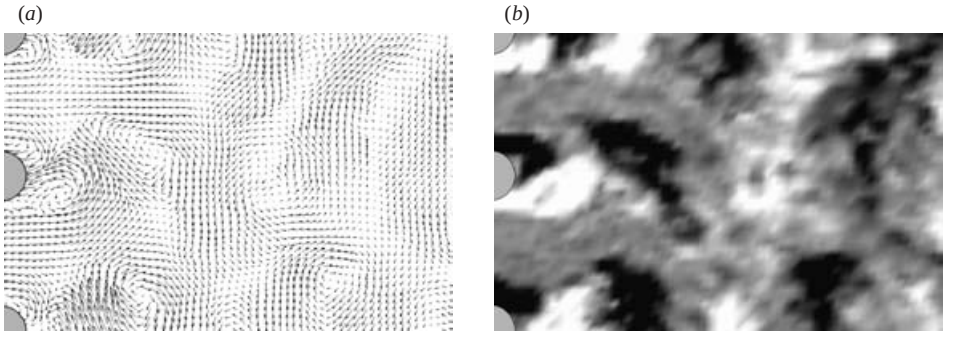

FIGURE 7. (*a*) Fluctuating velocity field downstream of a grid with 33% solidity, domain dimensions $0.75 \times 1.25\,\mathrm{m}^2$, experiment I. (*b*) Vorticity field obtained from the velocity field shown in (*a*). White indicates positive, grey zero, and black negative vorticity.

that the periodic vortex shedding is more strongly correlated in time for the shallow case than for the deepest case. The modulation is clearly visible for more than 10 s and is even visible at 2.5 m downstream. Apparently, the deeper water causes more irregularities in the flow through three-dimensional breakdown, prohibiting the formation of an organized flow pattern which is correlated over a long time. The large time scales present in the flow downstream of a 66% solidity grid are clearly recognized in the autocorrelation functions of figure 6(*b*). The strong modulations last a long time and account for more than 50% of the turbulent kinetic energy for that direction. The effect of the water depth on the shape of the spectra and correlation functions for a grid with 66% solidity (not shown) is not great, since the structures that are formed close to the grid already have a size comparable to or larger than the water depth. In both cases the eddies formed already feel the confinement of the flow. This was also clear from the spectra shown in figure 5(*d*). The separation between the large-scale motion and the small-scale turbulence is evident from the shape of the correlation function at small delays, ≈ 0.5 s. Especially in figure 6(*b*), the curve at $48D$ shows a fast drop related to the small-scale turbulence, followed by the slow modulation caused by the large-scale motion. The time resolution in this curve is 0.1 s. For that specific case the relative contribution of the large scales to the turbulent kinetic energy in the lateral velocity fluctuations can be estimated at $\approx 65\,\%$. It is self-evident that in all the curves of figure 6 the small-scale turbulence causes the sharp drop at small delays, although the effects are less pronounced when the disparity of both scales is not large.

4. Spatial properties

Using the PIV data spatial properties like vorticity and divergence of the flow field can be determined. The spatial resolution in this experiment is typically 2–3 cm, i.e. the small-scale turbulence properties are not properly resolved and only the large-scale motion at the free surface is captured. A typical example of the velocity field just downstream of the grid is given in figure 7(*a*). In this figure the global mean velocity has been subtracted from each vector to give an impression of the fluctuating component. The regular pattern of the eddies is clearly seen as well as the strong decrease of the intensity. The decrease in fluctuations is visualized in figure 8 where the homogeneity of the turbulent kinetic energy is demonstrated just downstream of

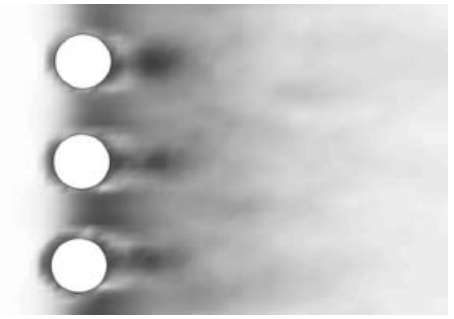

FIGURE 8. Distribution of the time averaged (30 s) turbulent kinetic energy in the horizontal plane.

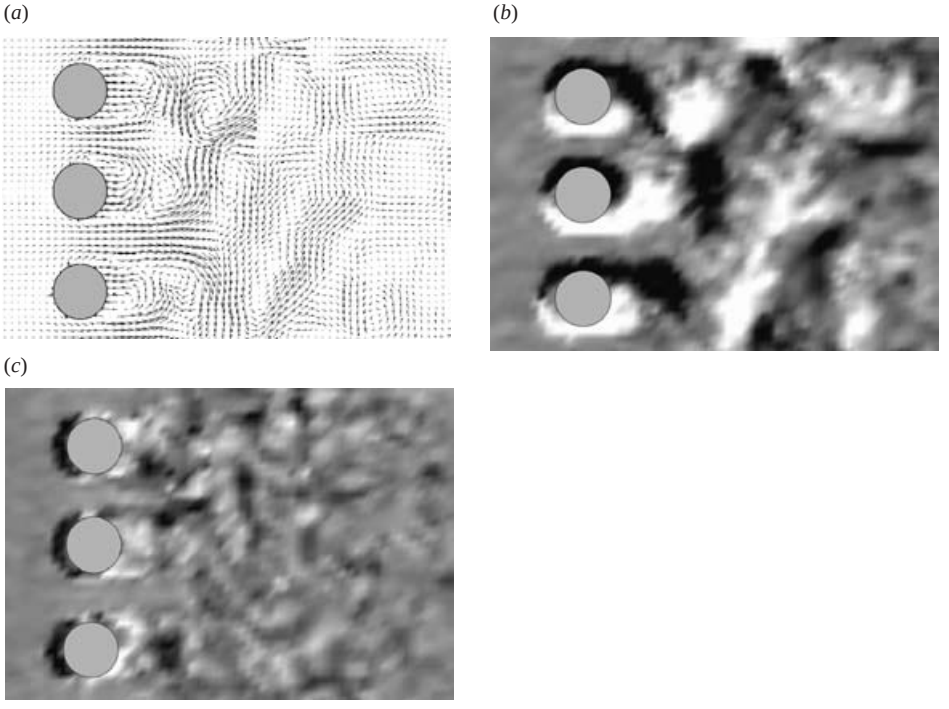

FIGURE 9. (*a*) Details of the PIV vector field around a grid of 50% solidity, in an area of $0.75 \times 1.25\,\mathrm{m}^2$, the arrows represent the flucutating velocity component, experiment II. (*b*) Vorticity field determined from the velocity field of (*a*). (*c*) Divergence of the instantaneous velocity field of (*a*).

the grid. Just downstream of the grid, the locations from which the eddies are shed are seen. A few cylinder diameters downstream this inhomogeneity disappears.

The eddying motions are better visualized by a plot of the vorticity, see figure 9(*b*). The clear light and dark patches represent the individual eddies with respectively positive and negative sense of rotation. In contrast with experiments where three-dimensional effects are virtually absent, like in stratified, rotational or soap film flows, no smooth and well-defined eddy structures are formed here. In order to determine the mean eddy size and shape at a certain location, an ensemble average should be

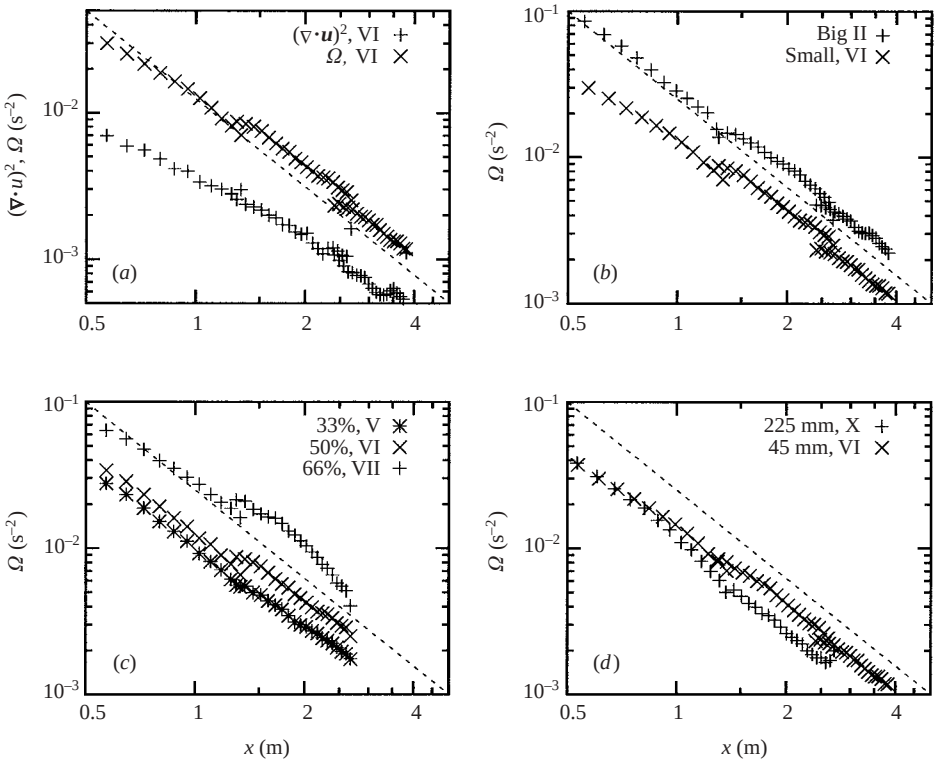

FIGURE 10. Enstrophy decay as a function of downstream distance obtained from the PIV data. (*a*) Comparison with the squared divergence. The line indicates a −2 slope. (*b*) The effect of cylinder diameter. (*c*) The effect of grid solidity. (*d*) The effect of water depth.

made of a large number of eddies that pass that location; the raggedness and the disturbances due to the small-scale turbulence and measurement noise then would disappear (van Prooijen, Booij & Uijttewaal 2000). Since the velocity field is measured in the horizontal plane at the free surface, three-dimensional effects are manifested in the divergence of the measured velocity field. From figure 9(*c*) it is seen that the areas of high divergence have no clear correlation with regions of high or low vorticity. The locations where the divergence of the velocity field is typically high are just in front and downstream of the cylinders. This suggests that three-dimensional effects are small and that experimental noise might be causing most of the divergence.

The phenomena can be made more quantitative by averaging the results, in particular the enstrophy $\frac{1}{2}\langle\omega_z^2\rangle$, over the lateral direction and over the recording time. The results are shown in figure 10 in which independent recordings from three different downstream areas are depicted. In this double logarithmic plot the decay of enstrophy closely follows a −2 slope over a substantial range of the distance. Within a small range all cases follow this slope quite closely. This characteristic of the large-scale motion can be recognized as a sign of two-dimensionality, as already predicted by Batchelor (1969).

It is interesting to see that the squared divergence of the flow field, plotted in the same figure as $\langle\partial u/\partial x + \partial v/\partial y\rangle^2$, follows a similar curve with significantly smaller values. The divergence is correlated to the enstrophy but only in the mean value. It was not possible to relate e.g. areas with high enstrophy to regions of high divergence,

which would have been the case if secondary circulation played an important role in the dynamics of large eddies. It is therefore concluded that the divergence as measured is dominated by small-scale turbulence and experimental noise. The values of the enstrophy and divergence measured in the undisturbed flow, i.e. without or far away from the grid, are $\langle \Omega \rangle \approx 10^{-3}\,\mathrm{s}^{-2}$ and $\langle (\nabla \cdot \boldsymbol{u})^2 \rangle \approx 5 \times 10^{-4}\,\mathrm{s}^{-2}$, respectively. These can be considered as an indication of the lowest values that can be detected with the PIV method used. The scatter in the curves is mainly due to the inaccuracy of the PIV method at the borders of the domains and the relatively short averaging time interval (30 s). The divergence can thus be used as an estimate for the accuracy in the determination of the enstrophy.

The effects of the parameters cylinder diameter, grid solidity and water depth are depicted in figure 10(b, c, d). An interpretation of the differences can only be made in a qualitative sense, since the enstrophy does not seem to obey a scaling similar to that found for the turbulent kinetic energy. It is shown in figure 10(b) that the rate of decay is similar for both cylinder diameters shown, whereas the absolute value of the enstrophy remains larger for the big cylinders. The effect of grid solidity is shown in figure 10(c), where remarkably the cases of 33% and 50% do not differ much while the 66% case yields much higher values. Finally, it is shown in figure 10(d) that the five-fold increase in water depth results in only a slightly faster enstrophy decay. This is in contrast to the clear differences in the energy density spectra and autocorrelation functions of figures 5(b) and 6(a). This might be an argument that the enstrophy decay should not be considered as a suitable indicator for the two-dimensionality of the flow.

In decaying *homogeneous* turbulence, the balance of turbulent kinetic energy $\frac{1}{2}\langle q^2 \rangle$ is relatively simple:

$$\frac{1}{2}\frac{\partial \langle q^2 \rangle}{\partial t} + \frac{\overline{U_i}}{2}\frac{\partial \langle q^2 \rangle}{\partial x_i} = -\overline{u_i u_j}\frac{\partial \overline{U_i}}{\partial x_j} - \overline{\epsilon}. \tag{4.1}$$

Turbulence decays downstream of the grid, yielding zero production of turbulent kinetic energy and not dependent on time. In this experiment the dissipation, as it is experienced by the large-scale horizontal motion, can be simplified to

$$\overline{\epsilon} = \nu_{eff}\,\omega_z \omega_z, \tag{4.2}$$

in which ν_{eff} is an effective 'eddy' viscosity. In the present case all the processes occurring on a scale smaller than the water depth will contribute to ν_{eff} as it is often used to model the effects of small-scale turbulence in a simple way. With the above simplifications the decay rate of the turbulent kinetic energy is directly coupled to the enstrophy Ω, i.e:

$$\frac{U}{2}\frac{\mathrm{d}\langle q^2 \rangle}{\mathrm{d}x} = -\nu_{eff}\,\Omega. \tag{4.3}$$

Considering the turbulence properties as given in figures 4 and 10(b), with energy decay that follows a -1.3 slope and enstrophy decay that follows a -2 slope, this effective viscosity is about 100 times as large as the molecular viscosity and is decreasing with downstream position. This concept of a subgrid-scale eddy viscosity has often been successfully applied to large-scale simulations of quasi-two-dimensional flows. A typical value for ν_{eff} that is related to the bottom boundary layer turbulence is straightforwardly estimated as $\nu_{eff} \approx \kappa u_* h/6 = \kappa \sqrt{c_f}\,\bar{U} h/6$, with κ the von Kármán constant and u_* the friction velocity. Though the order of magnitude of this estimate is correct, the proportionality with the water depth h is not convincingly reflected in

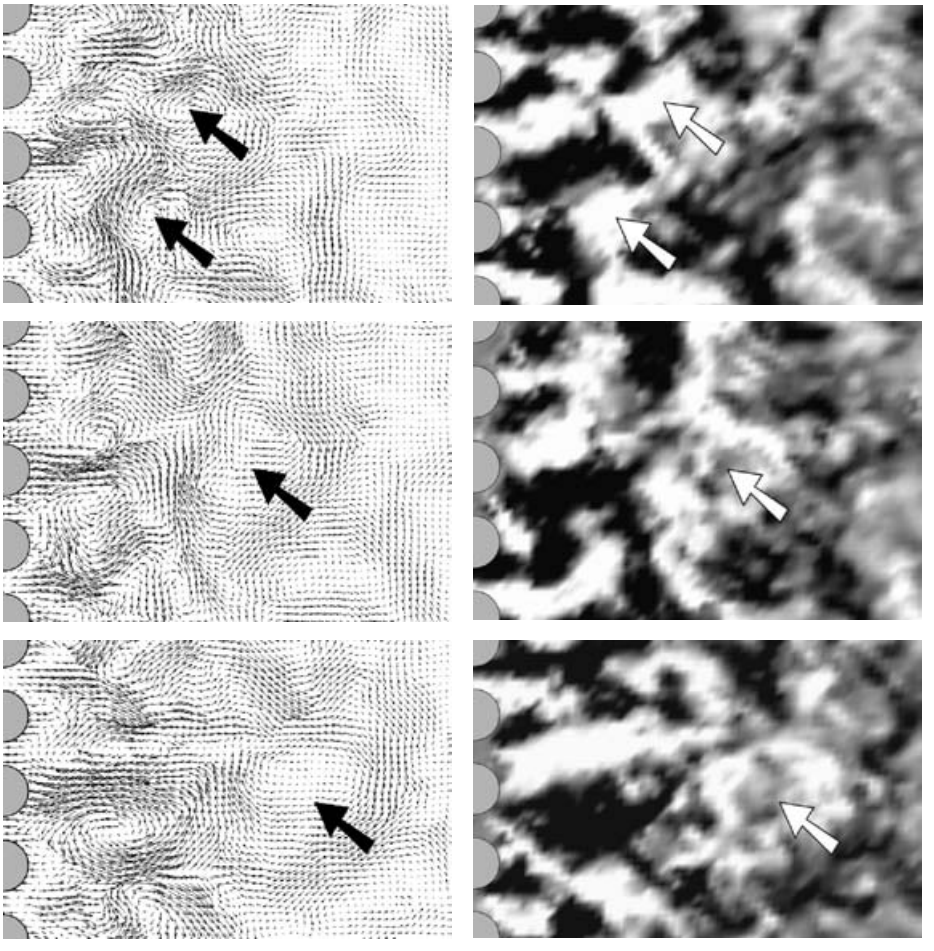

FIGURE 11. Vector fields (left) and vorticity (right) of two initially separated structures, indicated by arrows, that merge to a single larger one. The time interval between the top and the bottom figure is 8 s. For clarity the grey values for the vorticity have been inverted, i.e. white denotes negative vorticity and black positive. The area covered by the graphs is $1.1 \times 0.75\,\mathrm{m}^2$, water depth is 45 mm, and the grid consists of big cylinders with a 66% solidity, experiment III.

a significantly changed decay of the energy or the enstrophy for the five times deeper case of 225 mm (see figures 4*d* and 10*d*).

On the other hand, the shapes of the spectra in figures 5(*a*) and 5(*b*) indicate that the mechanism through which the energy in the large structures is lost does depend on the water depth. Apparently, the range of water depths used in this experiment is too small to be decisive regarding its influence on the turbulence dynamics as approximated by equation (4.3).

Another example of two-dimensional behaviour is given in the sequence of figure 11. It shows how two eddies emanating from different cylinder wakes form a larger structure. The vorticity patches are ragged and the structure that eventually is formed is not very clear. The combination of merging and decrease of intensity makes the interpretation somewhat problematic. The coarsening of the structures with downstream distance, as seen in the energy density spectra, is also reseen in the

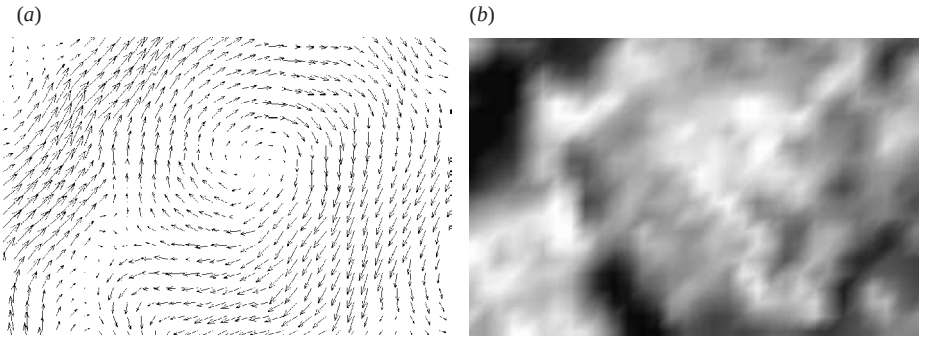

FIGURE 12. Snapshot of a large eddy 3 m downstream of the 66% solidity grid, 45 mm water depth, big cylinders, mean flow from left to right. (*a*) Velocity field and (*b*) vorticity field. The field of view is $1.1 \times 0.75\,\mathrm{m}^2$, the same as the previous figures.

velocity fields further downstream, see for example figure 12, where a huge structure has attained an in-plane area of $\approx 1\,\mathrm{m}^2$. It should be noticed that the intensity of vorticity in this case is an order of magnitude smaller than the vorticity just downstream of the grid. The squared divergence of this flow field does not give any indication of significant secondary motion, since its value has reached the background value of $5 \times 10^{-4}\,\mathrm{s}^{-2}$.

5. Concluding remarks

The experimental data presented in this paper demonstrate that shallowness alone will enforce two-dimensional features on the turbulence generated by a grid. The vertical confinement introduces a strong anisotropy in the turbulence scales of the order of, or larger than, the water depth, thus affecting the energy decay. The two-dimensionality is indicated by the following facts: a -3 slope in the energy density spectra, a growth of the characteristic length scales of the turbulence with increasing downstream distance, and indications of vortex merging. Thus, even in the absence of forcing by horizontal velocity gradients the dynamics of the large-scale turbulence appears to be analogous to the structures that are formed in shallow mixing layers, jets and wakes. Increasing the water depth causes a clear weakening of the two-dimensional features. Unfortunately, the water depth in the present experiments could not be increased further to enter the full three-dimensional regime. As with other investigations on shallow flow turbulence, the transition point where three-dimensional effects start dominating the turbulence decay has not been clearly identified.

Future experiments should be aimed at finding the conditions for the quasi-two-dimensional regime. At large water depths, three-dimensional instabilities will affect the large-scale dynamics, but at small water depths, where bottom friction dominates, three-dimensional effects play a role in prohibiting the development of large structures or even the shedding of vortices (Chen & Jirka 1995).

The authors are indebted to the Netherlands Organisation for Scientific Research (NWO) and the German Research Foundation(DFG) for sponsoring the collaboration between University of Karlsruhe and Delft University of Technology. V. Weitbrecht and C.F. Graf v. Carmer are gratefully acknowledged for their contributions to the experimental work.

REFERENCES

Adrian, R. J. & Yao, C. S. 1987 Power spectra of fluid velocities measured by laser Doppler velocimetry. *Exps. Fluids* **5**, 17–28.

Batchelor, G. K. 1969 Computation of the energy spectrum in homogeneous two-dimensional turbulence. *Phys. Fluids Suppl.* **II**, 233–239.

von Carmer, C. F., Koch, T. & Jirka, G. H. 2000 Grossräumige Wirbelstrukturen in turbulenter Flachwasserströmung. *Tech. Rep.* 766. Institut für Hydromechanik, Universität Karlsruhe (in German).

Chasnov, J. R. 1997 On the decay of two-dimensional homogeneous turbulence. *Phys. Fluids* **9**, 171–180.

Chen, D. & Jirka, G. H. 1995 Experimental study of plane turbulent wakes in a shallow water layer. *Fluid Dyn. Res.* **16**, 11–41.

Comte-Bellot, G. & Corrsin, S. 1966 The use of a contraction to improve the isotropy of grid-generated turbulence. *J. Fluid Mech.* **25**, 657–682.

Comte-Bellot, G. & Corrsin, S. 1971 Simple eulerian time correlation of full- and narrow-band velocity signals in grid-generated isotropic turbulence. *J. Fluid Mech.* **48**, 273–337.

Dracos, T., Giger, M. & Jirka, G. H. 1992 Plane turbulent jets in a bounded fluid layer. *J. Fluid Mech.* **241**, 587–614.

Fincham, A. M., Maxworthy, T. & Spedding, G. R. 1996 Energy dissipation and vortex structure in freely decaying, stratified grid turbulence. *Dyn. Atmos. Oceans* **23**, 155–169.

Fjortoft, R. 1953 On the changes in the spectral distribution of kinetic energy for two-dimensional, non-divergent flow. *Tellus* **5**, 225–230.

George, W. K. 1992 The decay of homogeneous isotropic turbulence. *Phys. Fluids* A **4**, 1492–1509.

Kraichnan, R. H. 1967 Inertial ranges in two-dimensional turbulence. *Phys. Fluids* **10**, 1417–1423.

Kumar, S., Gupta, R. & Banerjee, S. 1998 An experimental investigation of the characteristics of free-surface turbulence in channel flow. *Phys. Fluids* **10**, 437–455.

Lesieur, M. 1990 *Turbulence in Fluids*, 2nd edn. Kluwer.

Lumley, J. L. 1978 Decaying quasi-2D turbulence in a stratified fluid with circular boundaries. *Adv. Appl. Mech.* **18**, 123–176.

Martin, B. K., Wu, X. L. & Goldburg, W. I. 1998 Spectra of decaying turbulence in a soap film. *Phys. Rev. Lett.* **80**, 3964–3967.

Nezu, I. & Rodi, W. 1986 Open-channel flow measurements with a laser doppler anemometer. *J. Hydr. Engng* **112**, 335–355.

Nikora, V. 1999 Origin of the -1 spectral law in wall bounded turbulence. *Phys. Rev. Lett.* **83**, 734–736.

Pan, Y. & Banerjee, S. 1995 A numerical study of free-surface turbulence in channel flow. *Phys. Fluids* **7**, 1649–1664.

Paret, J. & Tabeling, P. 1997 Experimental observation of the two-dimensional inverse energy cascade. *Phys. Rev. Lett.* **79**, 4162–4165.

Perry, A. E., Henbest, S. & Chong, M. S. 1986 A theoretical and experimental study of wall turbulence. *J. Fluid Mech.* **165**, 163–199.

Pope, S. B. 2000 *Turbulent Flows*. Cambridge University Press.

van Prooijen, B. C., Booij, R. & Uijttewaal, W. S. J. 2000 Measurements and analysis methods of large scale horziontal coherent structures in a wide shallow channel. In *Proc. 10th Intl Symp. on Applications of Laser Techniques to Fluid Mechanics, Lisbon Portugal.*

van Prooijen, B. C. & Uijttewaal, W. S. J. 2002 A linearized model for the evolution of large-scale structures in shallow mixing layers. *Phys. Fluids* **14**, 4105–4114.

Riley, J. J. & Lelong, M.-P. 2000 Fluid motions in the presence of strong stable stratification. *Annu. Rev. Fluid Mech.* **32**, 613–657.

Sarpkaya, T. 1996 Vorticity, free surface, and surfactants. *Annu. Rev. Fluid Mech.* **28**, 83–128.

Sommeria, J. 1986 Experimental study of the two-dimensional inverse energy cascade in a square box. *J. Fluid Mech.* **170**, 139–168.

Taylor, G. I. 1935 Statistical theory of turbulence. *Proc. R. Soc. Lond.* A **151**, 421–444.

Townsend, A. A. 1956 *The Structure of Turbulent Shear Flow*. Cambridge University Press.

Uijttewaal, W. S. J. & Booij, R. 2000 Effects of shallowness on the development of free-surface mixing layers. *Phys. Fluids* **12**, 392–402.

Vorobieff, P., Rivera, M. & Ecke, R. E. 1999 Soap film flows: Statistics of two-dimensional turbulence. *Phys. Fluids* **11**, 2167–2177.

Walker, D. T., Leighton, R. I. & Garza-Rios, L. O. 1996 Shear-free turbulence near a flat free surface. *J. Fluid Mech.* **320**, 19–51.

Warhaft, Z. & Lumley, J. L. 1978 An experimental study of the decay of temperature fluctuations in grid-generated turbulence. *J. Fluid Mech.* **88**, 659–684.

Willert, C. E. & Gharib, M. 1997 The interaction of spatially modulated vortex pairs with free surfaces. *J. Fluid Mech.* **345**, 227–250.